LAMINAR SOOT PROCESSES (LSP) EXPERIMENT: FINDINGS FROM SPACE FLIGHT MEASUREMENTS

P.B. Sunderland, D.L. Urban and Z.G. Yuan
NASA Glenn Research Center, Cleveland, Ohio

C. Aalburg, F.J. Diez and G. M. Faeth
The University of Michigan, Ann Arbor, Michigan

INTRODUCTION

The present experimental study of soot processes in hydrocarbon-fueled laminar nonbuoyant and nonpremixed (diffusion) flames at microgravity within a spacecraft was motivated by the relevance of soot to the performance of power and propulsion systems, to the hazards of unwanted fires, and to the emission of combustion-generated pollutants. Soot processes in turbulent flames are of greatest practical interest, however, direct study of turbulent flames is not tractable because the unsteadiness and distortion of turbulent flames limit available residence times and spatial resolution within regions where soot processes are important. Thus, laminar diffusion flames are generally used to provide more tractable model flame systems to study processes relevant to turbulent diffusion flames, justified by the known similarities of gas-phase processes in laminar and turbulent diffusion flames, based on the widely-accepted laminar flamelet concept of turbulent flames [1-4]. Unfortunately, laminar diffusion flames at normal gravity are affected by buoyancy due to their relatively small flow velocities and, as discussed next, they do not have the same utility for simulating the soot processes as they do for simulating the gas phase processes of turbulent flames.

Local effects of buoyancy are small in the soot reaction region of practical turbulent flames; therefore, buoyant laminar diffusion flames can only provide a proper model flame system for turbulent flames to the extent that buoyancy does not affect soot processes. Unfortunately, soot particles are too large to diffuse like gas molecules and are primarily convected by local flow velocities; as a result, their behavior in buoyant and nonbuoyant diffusion flames is quite different [4-6]. This can be explained based on both measurements [7-12] and predictions [13,14]. In a buoyant flame, soot nucleation first occurs near the flame sheet, after which the soot convects inward to more fuel-rich regions before finally being swept out of the flame (passing from fuel-rich to fuel-lean conditions) near the flame tip. In contrast, in nonbuoyant flame, soot nucleation first occurs near the cool core of the flame, after which the soot particles are swept directly through the flame (passing from fuel-rich to fuel-lean conditions) at all points along the flame surface within the dividing streamlines. Thus, soot processes within buoyant and nonbuoyant laminar diffusion flames are very different, with results for nonbuoyant laminar diffusion flames representing soot processes of interest for practical turbulent flames (that generally are nonbuoyant due to their large flow velocities).

These differences between soot processes in buoyant and nonbuoyant laminar diffusion flames motivated the first phase of the present experiments which involved measuring soot properties within nonbuoyant laminar jet diffusion flames. These results were somewhat compromised, however, because the test flames had rather large residence times, and corresponding large radiative heat losses; this resulted in radiative quenching near the flame tip which caused tip opening phenomena and associated emissions of unburned fuel and soot along the axes of the flames. Such excessive radiative heat losses are not typical of practical turbulent diffusion flames; therefore, the present experiments emphasized conditions where the flames were nearly adiabatic. Similar to the original experiments of Refs. 15-20, the present measurements sought the shapes, the laminar smoke point properties and the soot properties of round nonbuoyant laminar jet diffusion flames.

EXPERIMENTAL METHODS

Apparatus. A sketch of the test apparatus appears in Fig. 1. The arrangement consisted of a laminar jet diffusion flame stabilized at the exit of a round fuel nozzle extending along the axis of a windowed cylindrical chamber. The chamber had a diameter of 400 mm, a maximum length of 740 mm and was capable of operating at pressures of 30-130 kPa. The chamber was filled with an O2/N2 mixture to provide the nominal composition of dry air (21 ± 1% O2 by volume) with total O2 consumption during a flame test less than 10%. The flames were ignited using a retractable hot wire. Two fuel nozzles were considered, having inside diameters of 0.8 and 0.4 mm. The larger jet exit velocities, u_o, for a given fuel flow rate, yielded characteristic flame residence times,

$$t_{ch} = 2L_f/u_o \tag{1}$$

where L_f is the luminous flame length, that were 4-16 times smaller than the conditions of Refs. 15-20. The reduced radiative heat losses yielded nearly-adiabatic flames.

Instrumentation. Laminar flame shapes were measured using a CCD video camera. Soot volume fractions and temperature distributions were measured using imaging techniques, deconvoluting laser extinction measurements for soot volume fractions, and deconvoluting two-line emission measurements to find soot temperatures and mixture fractions. Other measurements are described in Urban et al. [15].

RESULTS AND DISCUSSION

Flame Shapes. Flame shape predictions adopted the simplified approach of Lin et al. [17] yielding the following expression for the flame length:

$$L_f - L_o = (3C_f Sc/(8\pi\mu))\, \dot{m}/Z_{st} \tag{2}$$

where L_o is the virtual origin, C_f is an empirical coefficient to match measurements and predictions (C_f=1 (basic theory), =1.13 (soot-containing flame at the laminar smoke point, and =0.56 (soot-free flame)), Sc=0.76 is the Schmidt number, μ is the flame viscosity, $\dot{m}$ is the burner flow rate and Z_{st} is the mass fraction of the fuel in a stoichiometric mixture of the burner exit and ambient fluids (ambient fluid = air in the following). See Ref. 17 for the formulas for other flame properties.

A typical video flame image appears in Fig. 2; these conditions correspond to an ethylene/air flame for the 0.8 mm diameter burner at a pressure of 1/2 atm. This flame has a length of 109 mm and is very near the laminar smoke point but with no evidence of tip opening. A preliminary evaluation of the flame length prediction of Eq. (2) is illustrated in Fig. 3. Predictions on this figure are for smoke-point and soot-free flames, setting L_o=0, taking a mean value of μ for air at 1100 K for all the flames and using Z_{st}=0.0636 and 0.0602 for ethylene- and propane-fueled flames, respectively. The test conditions included two soot-emitting flames, several flames near the laminar smoke point, several soot-containing flames at flow rates smaller than laminar smoke point conditions, and one soot-free (blue flame). The comparison between measurements and the simplified flame length expression of Eq. (2) is remarkably good for soot emitting and laminar smoke point flames and for the soot-free flame. The other soot-containing flames fall between these limits, as expected.

Laminar Flamelet Concept. The laminar flamelet concept implies that laminar diffusion flames should have scalar gas properties that are only functions of the degree of mixing of the flow, typically represented by the local mixture fraction, for given burner exit and ambient conditions. These functions, called state relationships, are applied to turbulent diffusion flames, assuming that turbulent diffusion flames involve a collection of strained laminar flamelets. The

use of the laminar flamelet approximation is effective for buoyant and nonbuoyant soot-free flames, vastly simplifying predictions because only mixture fraction predictions are needed to find all scalar properties [1-4]. As noted earlier, however, similar state relationships are not found for soot properties in buoyant laminar diffusion flames due to soot path effects. The success of the simplified flame shape analysis discussed in connection with Figs. 2 and 3, suggests that the laminar flamelet concept might be valid for soot properties within nonbuoyant laminar diffusion flames. In particular, the simplified analysis shows that the variation of mixture fraction (and thus all scalar properties) as a function of *time* is identical for all soot paths from the burner exit to the surroundings. This also implies identical soot properties along all soot paths through the present nonbuoyant laminar diffusion flames, even when the burner flow is varied.

The potential for soot property state relationships was tested by considering maximum soot concentrations along various soot paths for experiments carried out on STS-83 and –94. These results are illustrated in Fig. 6 as ratios of maximum soot volume fractions for each path considered through a given flame to the average of all the paths through the same flame, for the four flames for these experiments where characteristic flame residence times were small enough to make radiative heat losses small. As anticipated from the simplified theory, maximum soot concentrations for all the paths through the flames, for given burner exit and ambient conditions, are essentially the same within experimental uncertainties. Given successful subsequent evaluation of the soot property state relationship concept from the STS-107 results, an important simplification for understanding, and modeling, practical soot-containing turbulent diffusion flames will be obtained.

ACKNOWLEDGMENTS

This research was supported by NASA Grant Nos. NAG3-2048 and NAG3-2404.

REFERENCES

1. Bilger, R.W., *Combust. Flame* 30:277 (1977).
2. Faeth, G.M. and Samuelson, G.S., *Prog. Energy Combust. Sci*. 12:305 (1986).
3. Sivathanu, Y.R. and Faeth, G.M., *Combust. Flame* 82:211 (1990).
4. Gore, J.P. and Faeth, G.M., *J. Heat Trans*. 110:173 (1988).
5. Sunderland, P.B. et al., *Combust. Flame* 96:97 (1994).
6. Law, C.K. and Faeth, G.M., *Prog. Energy Combust. Sci*. 20:65 (1994).
7. Sunderland, P.B. et al., *Combust. Flame* 100:310 (1995).
8. Lin, K.-C. et al., *Combust. Flame* 104:369 (1996).
9. Santoro et al., *Combust. Flame* 51:203 (1983).
10. Santoro et al., *Combust. Sci. Tech*. 53:89 (1987).
11. Puri, R. et al., *Combust. Flame* 92:320 (1993).
12. Puri, R. et al., *Combust. Flame* 97:125 (1994).
13. Spalding, D.B., *Combustion and Mass Transfer*, Pergamon, New York, Chapt. 10, 1979.
14. Mortazavi et al., AIAA Paper No. 93-0708, 1993.
15. Urban, D.L. et al., *AIAA J*. 36:1346 (1998).
16. Faeth, G.M., *Microgravity Combustion Science* (H.D. Ross, ed.), Academic Press, New York, p. 83, 2001.
17. Lin, K.-C. et al., *Combust. Flame* 116:415 (1999).
18. Lin, K.-C. and Faeth, G.M., *AIAA J*. 37:759 (1999).
19. Dai, Z. and Faeth, G.M., *Proc. Combust. Inst*. 28:2085 (2000).
20. Urban, D.L. et al., *Proc. Combust. Inst*. 28:1965 (2000).

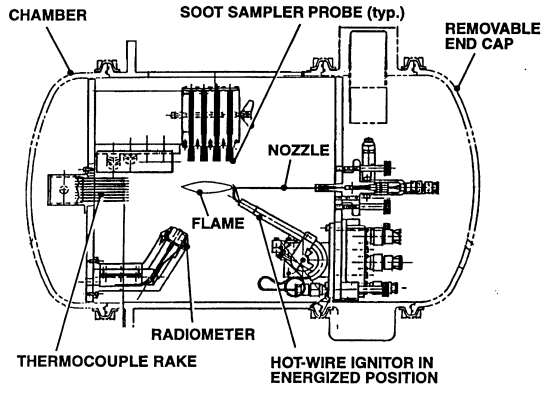

Fig. 1. Sketch of the Laminar Soot Processes (LSP) test apparatus for observations of nonbuoyant round laminar jet diffusion flames in still air at microgravity.

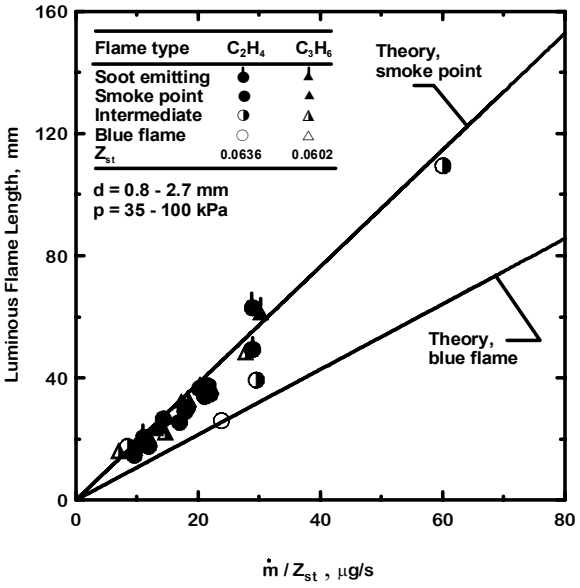

Fig. 3. Luminous flame lengths of round nonbuoyant and buoyant ethylene/air laminar jet diffusion flames as a function of fuel flow rate, burner diameter and pressure.

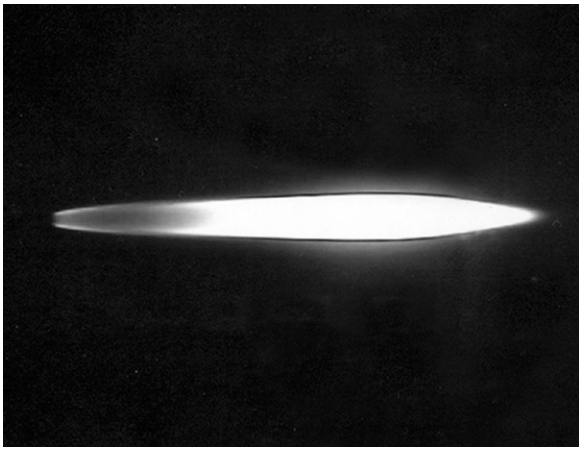

Fig. 2. Video image of a nonbuoyant round laminar jet diffusion flame in still air at microgravity (ethylene fuel jet from a 0.8 mm diameter burner port, pressure = 0.5 atm, maximum luminous flame length and diameter of 109 and 10 mm, respectively).

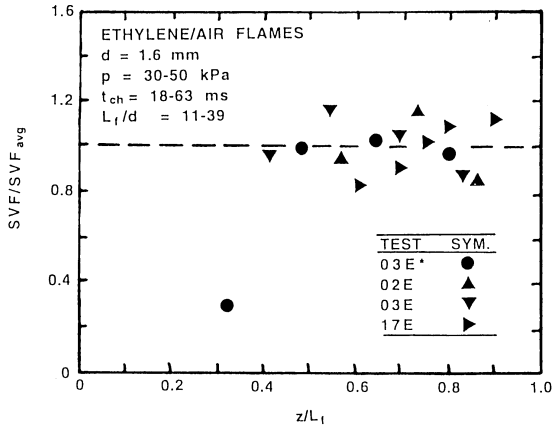

Fig. 4. Normalized maximum soot volume fractions as a function of normalized distance from the burner exit for round nonbuoyant ethylene/air laminar jet diffusion flames at microgravity.